International Journal of Concrete Structures and Materials

RESEARCH

Open Access

Factors Influencing Measurement of Dynamic Elastic Modulus from Disk-Shaped Concrete Specimen

Min Suk Kim[1], Jeong Jin Son[2], Chul-Woo Chung[2] and Chang Joon Lee[1*]

Abstract

The decrease in dynamic elastic modulus is a primary indicator of quantitative damage in concrete. To quantitatively assess depth-by-depth damage within a concrete structure, cylindrical specimens obtained through coring can be cut into disk specimens to measure the dynamic elastic modulus of concrete at each depth. To minimize external damage during coring, it is essential to extract cylinders with the smallest possible diameter. In addition, for higher resolution in depth-based damage assessment, creating disk specimens with the smallest possible thickness is necessary. However, there is no information available in the literature on experimental limitation of smallest possible diameter and thickness for dynamic elastic modulus of disk-shaped specimens. This study evaluated whether the dynamic modulus measured from various sizes of concrete disk specimens provided sufficient reliability compared to reference values obtained from cylinders. Moreover, the study examined how the presence of coarse aggregate and variation in the water–cement ratio significantly influenced the dynamic modulus measurement. In addition, test results from impulse excitation technique (IET) and impact resonance (IR) were compared to find a more reliable test method for dynamic elastic modulus of disk specimen. The experimental findings revealed that as the thickness-to-radius ratio of the disk specimens decreased, measured data variation increased. Mortar specimens without coarse aggregates showed less variability compared to concrete specimens, and the variation in dynamic modulus measured by IR was lower than that measured by IET.

Keywords Concrete, Disk, Dynamic elastic modulus, Impact resonance, Impulse excitation technique

1 Introduction

Recently, as deterioration in large-sized concrete structures causes loss of property and human life, a strong interest in developing tools to diagnose the exact extent of deterioration in structures has been initiated (Abu Shanab & Sorensen, 2023; Dvořák et al., 2023; Gharehbaghi et al., 2022; Ghodousian et al., 2023; Li et al., 2023; Shah et al., 2023; Yoon et al., 2021). It is because, in case of the partial damage, a more economic partial repair process can be chosen rather than rebuilding the entire structure after complete demolition. As the level of damage from deteriorated structure has been determined, the choice of appropriate repair procedure should have been followed.

Journal information: ISSN 1976-0485 / eISSN 2234-1315.

*Correspondence:
Chang Joon Lee
cjlee@cbnu.ac.kr
[1] Department of Architectural Engineering, Chungbuk National University, Chungdae-Ro 1, Seowon-Gu, Cheongju, Chungcheongbuk-Do 28644, Republic of Korea
[2] Division of Architectural and Fire Protection Engineering, Pukyong National University, Yongso-Ro 45, Nam-Gu, Busan 48513, Republic of Korea

For characterizing the level of deterioration, most of research works (Chen et al., 2023; Georgali & Tsakiridis, 2005; Hua et al., 2022; Kirchhof et al., 2015; Krishna et al., 2019; Lee et al., 2015, 2017; Ma et al., 2015; Thanaraj et al., 2020; Yang et al., 2009) have used full-sized cylindrical or prismatic specimens exposed to the specific deterioration environments, such as short-term and intensive conditions such as fire, or long-term and subtle conditions such as chloride penetration or irradiation. These studies measured parameters such as resonant frequency, wave velocity, weight/length change, and mechanical strength (if possible) of the specimens. This approach enables the characterization of concrete durability in specific environments because all necessary information, such as testing temperature, concentration, degree of exposure, and time, is clearly identified. However, regardless of the duration or magnitude of deterioration, the use of full-sized specimens does not accurately represent the damaging process of a real concrete structure. This is due to microcracks being generated from the point of origin of deterioration and propagating into the core of the concrete, leading to varying degrees of deterioration by depth. Since cumulative minor damage can compromise the integrity of the entire concrete structure, the first task for an engineer is to assess the extent of damage that have occurred within concrete structures to maintain the integrity of concrete structures and to extend their service life.

To assess the damage within concrete structures, it is necessary to understand the changes in material characteristics from the surface to deeper layers of the structure. For instance, when evaluating fire-induced damage, thermogravimetric analysis (Alarcon-Ruiz et al., 2005; Alqassim et al., 2016; Ingham, 2009; Lim et al., 2021; Mendes et al., 2009; Pathak et al., 2013; Ye et al., 2007) can be utilized. This analysis involves collecting small cement samples from various depths of the concrete surface and assessing the loss of chemically bound water as a function of depth. However, collection of the cement sample from concrete requires some level of expertise and often causes experimental error due to the differences in aggregate contents in the collected sample, thereby causing difficulties for on-site application. Another method, the depth of carbonation measured by phenolphthalein method (Byun & Ryu, 2017; Du et al., 2018; Ha et al., 2016; Li et al., 2013, 2014; Sim & Ryu, 2020), can also be utilized to evaluate pH of concrete samples taken at different depths. However, this method only indicates whether the pH of the concrete is below 9 or not. This method cannot provide any detailed information on how much damage has been occurred due to the fire (sample can be identified as undamaged if a small fraction of $Ca(OH)_2$ is available after fire damage). It is important to notice that these test procedures do not provide any information on residual mechanical properties of damaged concrete which are crucial for direct assessment of remaining service life.

When a depth-by-depth analysis on residual mechanical properties of concrete after deterioration needs to be performed, for example, the level of deterioration during fire or irradiation whose exposure conditions (heating rate, intensity, exposure time, etc.) are unclear, full-sized cylindrical core specimens cannot be used because bottom part of core specimen which is located away from the source of deterioration are not as damaged as upper part of core specimen which is located near the source of deterioration. For this reason, several attempts were made to utilize disk-shaped concrete specimens (sliced from cored concrete specimens) for estimation of mechanical properties of concrete. Leming et al., (1998) is one of the first research groups that have utilized disk specimens. They investigated the feasibility of fundamental frequency measurements to estimate the dynamic elastic modulus of the disk specimens, and found that dynamic elastic modulus of disk specimen could be accurately determined. Dilek and Reis () and Park and Yim () have also measured the dynamic elastic modulus of thin disk specimens after exposure to high temperature, demonstrating that the use of disk specimens with small depth increments enabled a depth-by-depth assessment of heat-induced damage in concrete. However, it is important to notice that all these studies employed disk specimens with a diameter of 100 mm and a thickness of 25 mm.

The diameter of the disk specimen can be determined by the diameter of the core drilling machine used to collect cylindrical concrete cores on-site. Since the collected core specimen needs to be eventually repaired, a smaller diameter of the core specimen is preferable. In addition, to obtain more detailed information on damage at different depths of the concrete, it is better to utilize thinner disk specimens. In summary, to obtain more detailed information on depth-by-depth damage, it is recommended to use the disk specimens with the smallest possible diameter and thickness. At this moment, there is no information available for actual (experimental) limitation of diameter and thickness that can be applicable for dynamic modulus of disk-shaped specimens. In fact, utilization of such thin disk specimens with smaller possible diameter can induce higher experimental variation. Therefore, the study evaluated whether the dynamic modulus measured from various sizes of concrete disk specimens, with diameters of 100 mm or less and thicknesses of 25 mm or less, provided sufficient reliability compared to reference values obtained from cylinder measurements.

Table 1 Chemical composition of ordinary Portland cement

Composition	CaO	SiO_2	Al_2O_3	MgO	Fe_2O_3	SO_3	K_2O	TiO_2	L.O.I
(%)	64.4	18.85	5.62	3.65	3.06	2.53	1.04	0.41	0.44

Table 2 Physical properties of aggregate

Properties	Specific gravity (g/cm^3)	Absorption (%)	Fineness modulus/maximum size (mm)	Bulk density (%)
Fine aggregate	2.56	1.73	2.8	1.70
Coarse aggregate	2.59	0.67	25	1.67

Table 3 Mix proportions of concrete

Sample	Unit weight (kg/m^3)				
	W/C	Water	Cement	Fine aggregate	Coarse aggregate
C35 [1 m^3]	0.35	170	485.71	696.87	1045.3
M35 [0.597 m^3]		170	485.71	696.87	–
M35 [1 m^3]		284.89	813.96	1167.82	–
C50 [1 m^3]	0.5	170	340	744.57	1116.85
M50 [0.569 m^3]		170	340	744.57	–
M50 [1 m^3]		298.70	597.41	1308.27	–

NOTE: Total volume of M35 [0.597 m^3] and M50 [0.569 m^3] mix proportions were recalculated to meet total volume of 1 m^3

Two different types of concretes, high strength and normal strength concretes with water-to-cement ratios of 0.35 and 0.50, were prepared for measurements. Disk specimens with various thickness-to-radius ratio (t/r) were prepared, and dynamic elastic modulus measured by impulse excitation and impact resonance methods were compared. The effect of coarse aggregate on dynamic elastic modulus of disk specimens, which can be one of the crucial factors that can determine the smallest possible diameter and thickness, was also investigated using mortar disk specimens. Consistency, variability, and validity of the experimental results obtained from disk specimens with varying diameters and thicknesses are analyzed, and general suggestions on a successful measurement of dynamic elastic modulus of disk-shaped concrete specimen are discussed.

2 Experimental Procedure

2.1 Materials

In this study, ordinary type I Portland cement was used for fabrication of concrete specimens. Chemical compositions of ordinary Portland cement, measured by X-ray fluorescence (XRF), are presented in Table 1. Natural sand and crushed stone were used as fine and coarse aggregate, respectively. Physical properties of fine and coarse aggregate were measured following ASTM C 128 standard test method for relative density (specific gravity) and absorption of fine aggregate, and are summarized in Table 2. Polycarboxylate-based superplasticizer was used to obtain necessary slump range of 100 mm.

2.2 Mixing and Placing

Mix proportion of concrete used in this work is presented in Table 3. Mix proportion was designed to understand the effect of w/c and the presence of coarse aggregate on the difference in dynamic elastic modulus of cylindrical concrete specimen and concrete disk specimen. In Table 3, C series (C35 and C50) are concrete and M series (M35 and M50) that coarse aggregates were removed from mix design. Unit water content was fixed at 170 kg/m^3 to control total solid content the same between C35 and C50 (considering that the amount of total solid content affects elastic modulus). Fine aggregate to overall aggregate ratio was also fixed at 0.4.

Mixing of concrete and mortar was performed using a medium-sized concrete pan mixer with a mixing volume of 60 L. When mixing, cement and aggregate were first added and dry mixed for 30 s. Water was poured and mixed for 90 s at 30 rpm. After mixing was completed, concrete and mortar were poured into cylindrical molds of ϕ100×200 mm, ϕ 75×150 mm, and ϕ 50×100 mm, respectively. Samples were placed into the mold in 3 layers, and rodded 25 times and vibrated 15 times with rubber mallet to obtain well-consolidated specimen. Specimens were sealed with plastic wrap to prevent evaporation of water and cured at the ambient temperature of 21 ± 2 °C for 24 h. The specimens were demolded after a day, and placed in 21 °C saturated lime solution until the age of 28 days in a water bath. At 28 days, concrete specimens were taken out for measurement of dynamic elastic modulus. The 28-day compressive strengths of C35 and C50 concretes were measured following ASTM C 39 standard test method for compressive strength of cylindrical concrete specimens. Those were 65.8 and 52.4 MPa, respectively. Experimental plan and sample

preparation procedure are presented as a flow chart in Fig. 1, and explained at following sections in detail.

2.3 Dynamic Elastic Modulus of Cylindrical Specimen

Prior to cutting the cylindrical specimen into disk specimens, the dynamic elastic modulus of the cylindrical specimen was measured using ASTM C215 (AMERICAN SOCIETY FOR TESTING AND MATERIALS, 2019). The schematic of the test setup is shown in Fig. 2. The cylindrical specimen was placed on a soft polyurethane sound absorbing foam to make specimen in free-end boundary condition. A PCB-353B15 accelerometer (PCB Piezotronics Inc., USA) was attached to the center of one end, and the center of the other end was impacted using a rod with 5 mm diameter iron ball to produce a longitudinal impact wave. The acceleration signal that was measured by accelerometer was amplified through PCB-480B21 signal conditioner (PCB Piezotronics Inc., USA), and the data were obtained using NI-USB-3152 high-speed digital oscilloscope (National Instrument Inc., USA).

Obtained data in the time domain were converted into a frequency domain signal using fast Fourier transform (FFT). The natural resonance frequency was obtained from the frequency domain signal. Using the natural

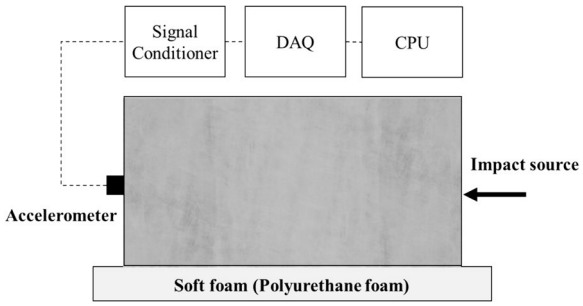

Fig. 2 Schematic illustration on fundamental longitudinal frequency measurement of the cylindrical specimen

resonance frequency, the dynamic elastic modulus of the cylindrical specimen was calculated using Eq. (1):

$$E = 5.093\left(L/d^2\right)Mn^2, \tag{1}$$

where L is the length of specimen, d is the diameter of cylinder, M is the mass of, n is the resonance frequency, and E is the dynamic modulus of elasticity.

2.4 Preparation of Disk Specimens

Disk specimens with 4 different various thickness-to-radius ratios (t/r; 0.2, 0.3, 0.4, and 0.5) were produced by

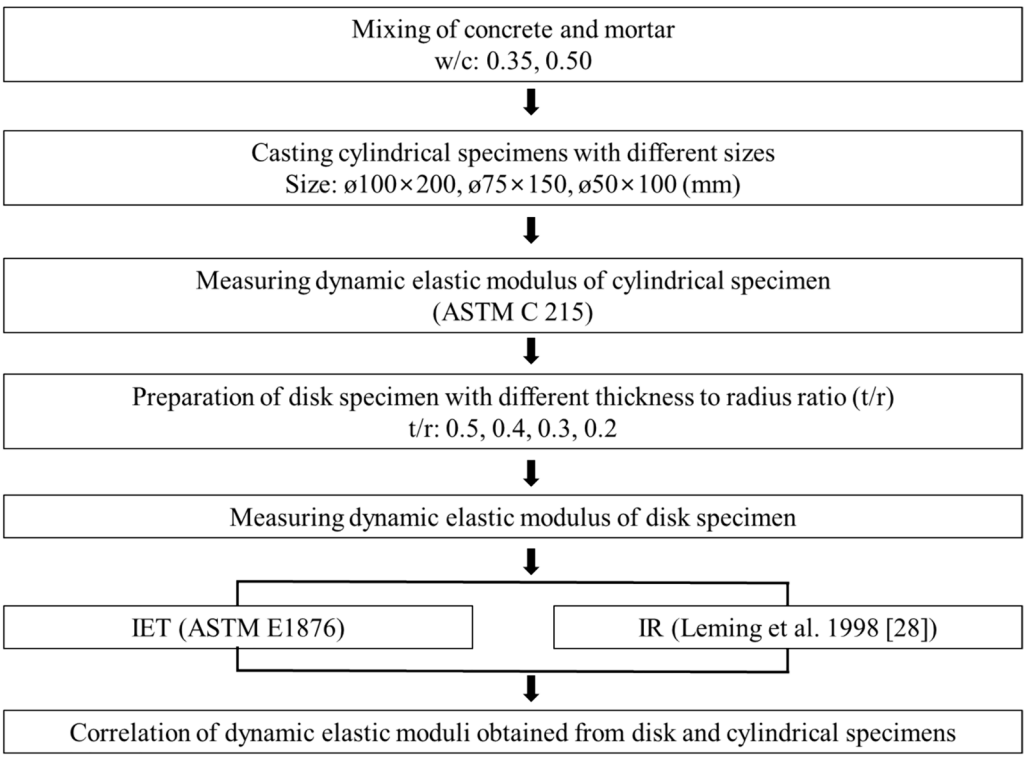

Fig. 1 A flow chart for experimental program used in this work

slicing cylindrical concrete and mortar specimens. For 100 mm diameter cylindrical specimens, disk specimens with diameter of 10, 15, 20, and 25 mm (corresponding t/r radios of 0.2, 0.3, 0.4, and 0.5) were prepared. For 75 mm and 50 mmm diameter cylindrical specimens, disk specimens with diameter of 7.5, 11.25, 15, and 18.75 mm and 5, 7.5, 10, and 12.5 mm were prepared, respectively. The types and numbers of disk specimens used for estimation of dynamic elastic modulus are shown in Table 4.

2.5 Dynamic Elastic Modulus of Disk Specimen

2.5.1 Impulse Excitation Technique

The dynamic elastic modulus of the concrete disk specimen was measured using impulse excitation technique (IET) specified in ASTM E1876-01 (AMERICAN SOCIETY FOR TESTING AND MATERIALS, 2022). This method utilizes the ratio of resonant frequencies of two different vibrating modes and the geometric information of the disk specimen to estimate the Poisson's ratio and the dynamic elastic modulus of the disk specimen.

Table 4 Type and numbers of specimens used in this work

Type	Diameter			
	50 mm	75 mm	100 mm	Total (EA)
Cylinder	8	8	8	24
Disk	48	48	48	144

The test setup for IET is shown in Fig. 3. The same impactor, accelerometer, signal conditioner, and digital oscilloscope were utilized for measurements. The four supports were arranged at 90-degree intervals on a concentric circle with a diameter equal to 0.681 times the diameter of the specimen. The disk specimens were mount on the supports. Then, an acceleration signal was recorded at point S1 by exciting point X1 with a steel ball. The time domain acceleration signal was transformed into a frequency domain by FFT, and the first resonance frequency was obtained. Similarly, the second resonance frequency was obtained with the acceleration signal measured at point S2 by exciting point X2.

The dynamic elastic modulus of the disk specimen was calculated with Eq. (2) using the resonance frequencies measured by IET:

$$E = (E_1 + E_2)/2, \tag{2}$$

where $E_i = [37.6991 f_i^2 D^2 m(1-\mu^2)](K_i^2 t^3)$, f_i is the i-th natural resonance frequency, D is the diameter of disk, m is the mass of disk, μ is the Poisson's ratio, K_i is the geometric factor for the i-th natural resonance frequency, and t is the disk thickness. The Poisson's ratio μ and geometric shape factor K_i can be obtained from ASTM E1876-01.

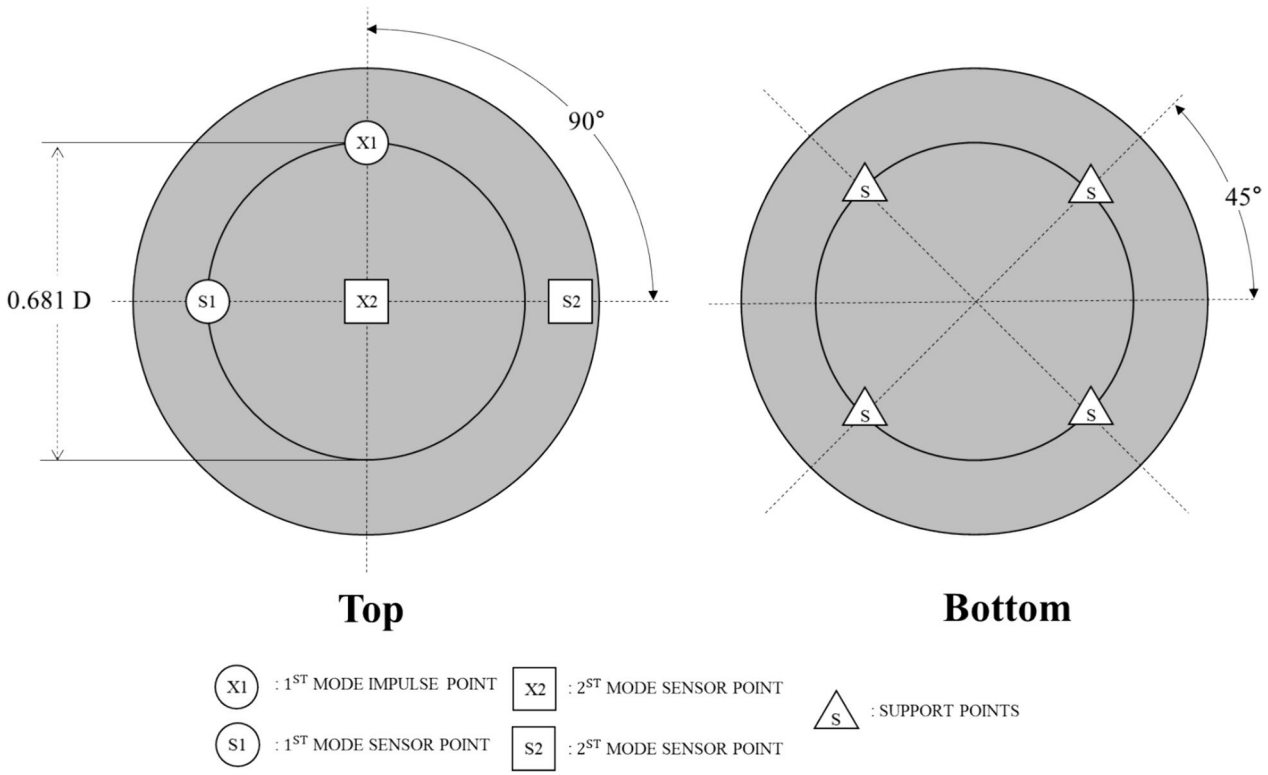

Fig. 3 Schematic figure of impulse excitation technique

2.5.2 Impact Resonance Method (IR)

The dynamic elastic modulus of the concrete disk specimens was measured using impact resonance (IR) method proposed by Leming et al. (1998). The IR method measures the resonant frequency of a disk specimen with a free-end boundary condition and estimate the dynamic elastic modulus using the frequency. The schematic of the testing setup is shown in Fig. 4. Disk specimens were placed on a soft polyurethane foam to set a free-end boundary state. An accelerometer was place at the center of the top surface of the disk specimen. Near the center of the disk specimen was excited with an iron ball impactor. The acceleration was measured as a function of time and converted into a frequency domain signal using FFT. From the frequency domain signal, the natural resonant frequency of the disk specimen was obtained.

The dynamic elastic modulus of the disk specimen was determined using Eq. (3):

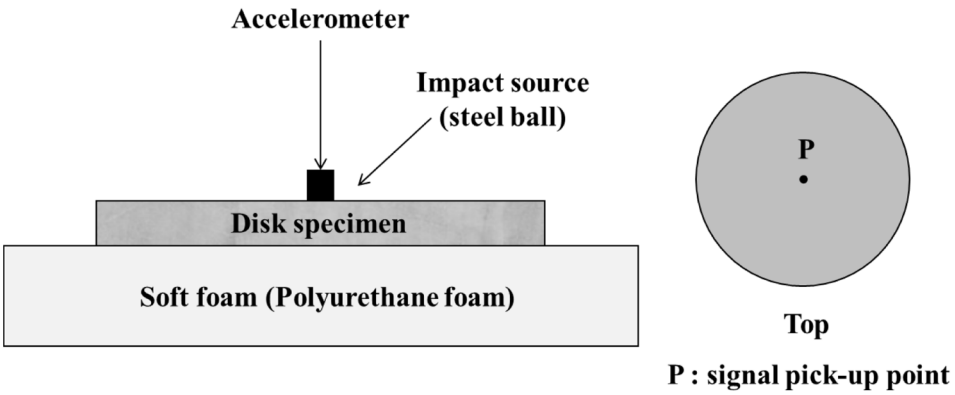

(a)

(b)

Fig. 4 Test configuration for impact resonance method: **a** schematic illustration and **b** photographic image

Table 5 Frequency parameter Ω_0 for different t/r ratio and Poisson's ratio

t/r ratio	Poisson's ratio						
	0.15	**0.175**	**0.2**	**0.225**	**0.25**	**0.275**	**0.3**
0.2	0.7225	0.7385	0.7545	0.7715	0.7785	0.8065	0.8255
0.3	1.0285	1.0495	1.0715	1.0945	1.1185	1.1425	1.1675
0.4	1.2855	1.3125	1.3385	1.3655	1.3935	1.4225	1.4515
0.5	1.4995	1.5285	1.5585	1.5895	1.6205	1.6525	1.6855

$$E_d = 2(1+\nu)\rho\left(\frac{\pi f d}{\Omega_0}\right)^2, \quad (3)$$

where ν is the Poisson's ratio of the disk, ρ is the density of the disk, f is the measured natural resonance frequency of the disk, d is the diameter of the disk, and Ω_0 is the frequency parameter associated with the fundamental mode of vibration. The frequency parameter Ω_0 can be determined by the plate theory based on the axisymmetric flexural vibration of thick free circular plate (Hutchinson, 1979; Martinček, 1965). A MATLAB (Works & Inc, 2020a) code was developed to determine frequency parameter Ω_0 based on the details described in the work of Leming et al. (1998). The calculated frequency parameters Ω_0 for different Poisson's ratio and disk thickness/radius ratio are shown in Table 5.

2.6 Correlation Analyses

A correlation analysis was performed using Pearson's correlation coefficient to quantitatively confirm the effect of various factors on the degree of difference between the dynamic elastic modulus of cylindrical and disk specimen. A commercial spreadsheet program (Excel, Microsoft Co. Ltd. USA) was used for correlation analysis, and the significance level (p) was set at 0.05. The variables used for correlation analysis were the diameter of the disk specimen, t/r ratio, ratio of dynamic elastic modulus (E_{disk}/E_{cyl}) between the disk and cylindrical specimen, and the standard deviation of E_{disk}/E_{cyl}.

2.7 Statistical Analyses

The statistical analysis (paired t-test) was performed using a commercial spreadsheet program (Excel, Microsoft Co. Ltd. USA). The "t-test" was applied on the sets of E_{cyl} and compared with the sets of E_{disk}. The confidence level of 95% was chosen, and the null hypothesis was set as E_{cyl} was identical to E_{disk}. The null hypothesis was accepted if the p value was above 0.05. When the p value was less than 0.05, the null hypothesis was rejected meaning that E_{cyl} is different from E_{disk}.

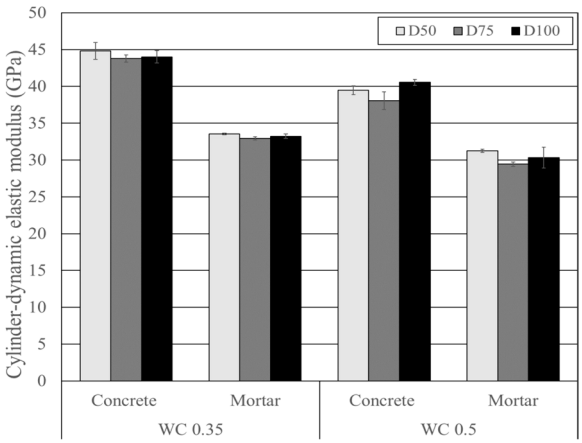

Fig. 5 Dynamic elastic moduli of cylindrical concretes

3 Results and Discussion

3.1 Dynamic Elastic Modulus of Cylindrical Specimen

Fig. 5 and Table 6 show dynamic elastic modulus of cylindrical specimens with varying w/c and aggregate contents. According to Fig. 5, concrete with lower w/c showed higher dynamic elastic modulus although the same unit water content was used to make concrete specimens. Since unit water content was fixed at 170 kg/m^3 for both w/c 0.35 and 0.50 concretes, the reduction of w/c from 0.5 to 0.35 led to the increase in the binder content with decrease in aggregate content. Since the elastic modulus of aggregate is higher than that of cement paste (Bang et al., 2013; Mitchell et al., 2014), reduction in the aggregate content in w/c 0.35 concrete (see Table 3) could have decreased the dynamic elastic modulus of concrete, showing almost no difference compared to that of w/c 0.50 concrete which had higher aggregate content (Table 3). However, it was found that dynamic elastic moduli of w/c 0.35 concretes were approximately 12% higher than those of w/c 0.50 concretes. Such an increase should have been related to the enhancement of microstructure in w/c 0.35 concrete compared to that of w/c 0.50 concrete. In w/c 0.35 concrete, higher amount of water has been consumed for hydration of cement,

Table 6 Dynamic elastic moduli of entire specimens (GPa)

			50 mm diameter				75 mm diameter				100 mm diameter			
Cylinder ASTM C 215		C35	44.83				43.76				44.01			
		M35	33.53				32.94				33.24			
		C50	39.48				38.06				40.55			
		M50	31.27				29.43				30.31			
Specimen			**Thickness/radius**											
			0.5	**0.4**	**0.3**	**0.2**	**0.5**	**0.4**	**0.3**	**0.2**	**0.5**	**0.4**	**0.3**	**0.2**
Disk	IET method	C35	48.02	34.92	41.16	48.59	52.34	48.47	62.62	62.29	40.55	50.43	51.62	40.55
		M35	30.30	27.43	30.14	29.73	31.60	25.17	29.20	35.44	32.13	30.46	33.56	33.71
		C50	30.98	31.07	38.71	32.44	52.09	44.34	52.38	67.14	39.37	49.59	52.22	48.31
		M50	24.73	25.51	30.02	25.12	28.53	29.64	26.02	28.74	28.39	26.51	26.05	28.51
	IR method	C35	47.10	39.22	44.22	58.73	47.97	52.17	47.28	50.38	41.55	49.87	46.27	41.55
		M35	33.63	32.17	34.13	12.45	33.13	34.32	31.48	31.05	34.32	32.42	33.53	26.80
		C50	34.87	34.53	40.73	47.48	41.98	43.22	44.93	46.30	39.52	46.95	46.80	42.87
		M50	29.62	29.55	34.20	10.97	30.27	31.25	28.70	25.92	30.92	31.83	28.42	26.97

and higher reduction in porosity caused densification of interfacial transition zone (ITZ) that strongly affects elastic modulus of concrete as third phase material (Nilsen & Monteiro, 1993).

The work done by Bharatkumar et al., (2001) is a good example case to compare because their work used the same water to binder ratios (0.35 and 0.50) while maintaining the unit water content (170 kg/m^3) the same for both w/b 0.35 and 0.50 concretes. Similar results were observed from the work of Bharatkumar et al., (2001) that the static elastic modulus of concrete with w/c 0.35 (around 45 GPa) was approximately 22% higher than that of w/b 0.35 concrete around 35 GPa). Higher difference in elastic modulus (approximately 22%) between w/b 0.35 and 0.50 compared to this work (approximately 12%) was associated with the nature of testing: static elastic modulus for the work of Bharatkumar et al., (2001) and dynamic elastic modulus for this work. The effect of ITZ in elastic modulus should be more significant in static measurement because test runs until the breakage of the specimen. Dynamic measurement was less affected by the presence of ITZ because it uses small amount of impact energy that cannot cause failure of ITZ (Zhang et al., 2018; Zhou et al., 2021).

According to Fig. 5, the difference in dynamic elastic modulus between concrete and mortar specimens was greater than that caused by the increase of w/c. approximately 25% and 23% reduction in dynamic elastic modulus was observed for w/c 0.35 and 0.50, respectively. It should be noted that mortar specimens were prepared by excluding the coarse aggregate content (see Table 3). As a result, the amount of water, cement, and fine aggregate were proportionally increased to fill the volume of coarse aggregate. Since higher unit water content (170–284.89 kg/m^3 for w/c 0.35, 170–298.70 kg/m^3 for w/c 0.50) increased the amount of water filled capillary porosity, dynamic elastic modulus of mortar should have been decreased. Proportional reduction in total aggregate volume (from 67.58% in concrete to 45.62% in mortar for w/c 0.35 specimens and from 72.20% in concrete to 51.10% in mortar for w/c 0.5 specimens) was another significant reason for the reduction in dynamic elastic modulus. It is worth noting that dynamic elastic modulus of w/c 0.35 mortar specimen was approximately 16% lower than that of w/c 0.50 concrete. Such result verified the significance of aggregate proportion in dynamic elastic modulus of concrete.

3.2 Dynamic Elastic Modulus of Disk Specimen

For comparison of dynamic elastic modulus of disk specimen with that of cylindrical specimen, dynamic elastic modulus of disk specimens obtained from Eqs. (2) and (3) were divided by dynamic elastic modulus of cylindrical specimens that was shown in Table 1, and expressed as ratio (E_{disk}/E_{cyl}) between dynamic elastic modulus of disk specimen (E_{disk}) and cylindrical specimen (E_{cyl}). The obtained values with 3 different diameters and 4 different t/r (thickness-to-radius)

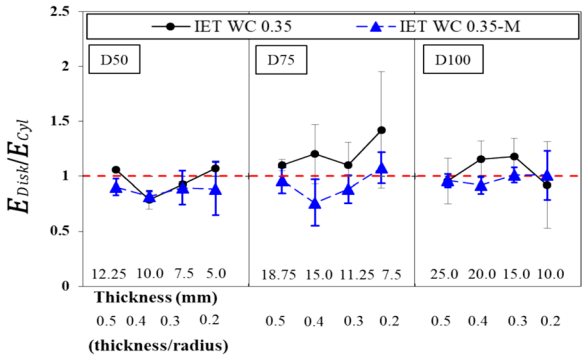

Fig. 6 Ratio of dynamic elastic modulus of w/c 0.35 disk and cylinder (E_{disk}/E_{cyl}) measured by IET

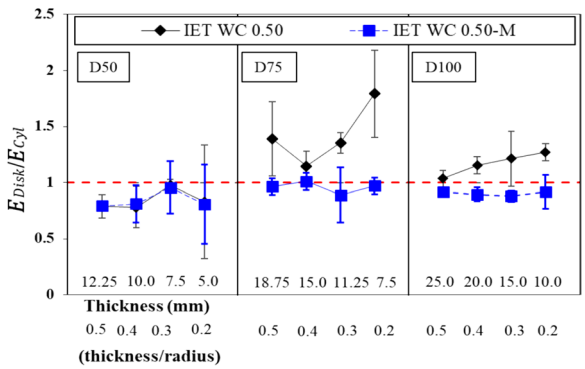

Fig. 7 Ratio of dynamic elastic modulus of w/c 0.50 disk and cylinder (E_{disk}/E_{cyl}) measured by IET

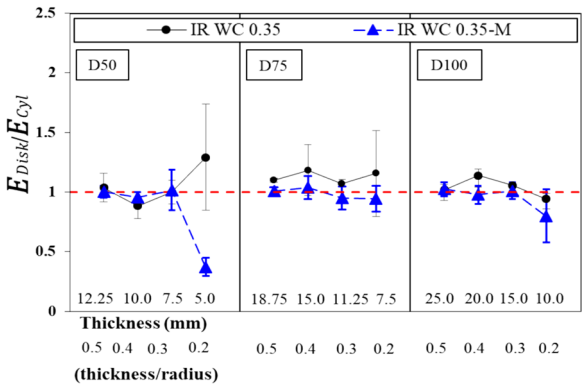

Fig. 8 Ratio of dynamic elastic modulus of w/c 0.35 disk and cylinder (E_{disk}/E_{cyl}) measured by IR

ratios are presented in Figs. 6 and 7 (measured by IET) and Figs. 8 and 9 (measured by IR), respectively. The error bars in figures mean the standard deviation of the values, which represent the variability of the estimated value of the dynamic elastic modulus.

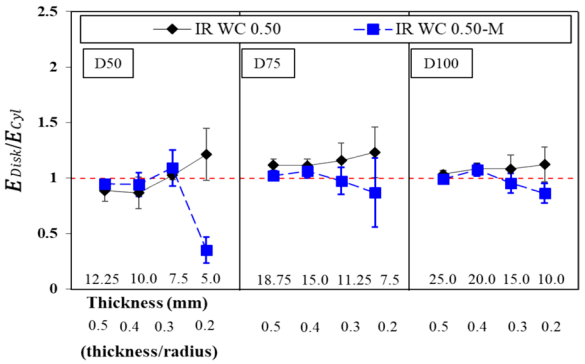

Fig. 9 Ratio of dynamic elastic modulus of w/c 0.50 disk and cylinder (E_{disk}/E_{cyl}) measured by IR

3.2.1 Dynamic Elastic Modulus by IET

Fig. 6 shows ratio of E_{disk}/E_{cyl} (measured by IET) of w/c 0.35 concrete and mortar obtained from various t/r ratio with varying size of diameter. Regardless of the disk diameter, dynamic elastic modulus of disk specimens with larger t/r (thickness became thicker) showed closer values to dynamic elastic modulus of cylindrical specimen (E_{disk}/E_{cyl} stays closer to the line of equality). As t/r ratio decreases (thickness became thinner), variation in data became greater meaning that the data cannot be as credible as that obtained from thicker disk specimens. It should be noted that the variation of data was significantly reduced when diameter of the disk specimen was 100 mm. In general, thicker disk specimens with larger diameter showed more stable data. Mortar specimens generally showed lower E_{disk}/E_{cyl} than concrete specimens, but overall trend was similar to that of concrete specimens.

Fig. 7 shows ratio of E_{disk}/E_{cyl} (measured by IET) of w/c 0.50 concrete and mortar. In case of w/c 0.50 specimens, the effect of larger t/r on E_{disk}/E_{cyl} was unclear. However, it was clear that variation in data was reduced when t/r ratio increases. The stability of data was the highest when 100 mm diameter disk was utilized for the measurement. The effective t/r to obtain stable measurement was 0.5 (thickness of 25 mm). It is because, although the variation in data was not so much changed, the dynamic modulus of disk specimen continued to increase as thickness of the specimen decreased (t/r ratio decreased). In general, mortar specimens showed more stable measurement than concrete specimens. It is strongly associated with the variation in coarse aggregate proportion in each of the disk specimen that occurred by thickness of the disk being smaller than the maximum size of coarse aggregate.

For both w/c 0.35 and 0.50 concrete disk specimens, disk specimens with diameter of 75 mm showed much

higher dynamic elastic modulus than that of cylindrical specimens. The variation in data was also greater than disk specimens with other diameters. Disk specimens with 75 mm diameter showed completely different behavior compared to those of disk specimens with 50 mm and 100 mm diameters. In case of IET, no specific trend (data variation, accuracy, etc.) was found regarding the size of the diameter. The reason is unclear at this moment.

3.2.2 Dynamic Elastic Modulus by IR

Fig. 8 shows ratio of E_{disk}/E_{cyl} (measured by IR) of w/c 0.35 concrete and mortar obtained from various t/r ratio with varying size of diameter. Except for the case of 50 mm diameter mortar disk specimen with $t/r=0.2$ (thickness of 5 mm), dynamic elastic modulus of disk specimen did not show great difference compared to that of cylindrical specimen. Similar to the case of IET, dynamic elastic modulus of disk specimens with larger t/r (thickness became thicker) showed closer values to dynamic elastic modulus of cylindrical specimen (E_{disk}/E_{cyl} stays closer to the line of equality). In general, disk specimens with larger diameter tended to show less variation in data. Variation in data became also greater as t/r ratio decreases, but level of variation was lower than that measured by IET. E_{disk}/E_{cyl} of mortar specimens did not exactly follow that of concrete specimens, but the differences in data measured by IR was smaller than those measured by IET.

Fig. 9 shows ratio of E_{disk}/E_{cyl} (measured by IR) of w/c 0.50 concrete and mortar obtained from various t/r ratio with varying size of diameter. Similar to the case of w/c 0.35, 50 mm diameter disk specimen with $t/r=0.2$ (thickness of 5 mm) showed much less dynamic elastic modulus than that of cylindrical specimen. Such a great difference could have been associated with poor preparation or damage associated with the preparation of thin disk specimen. Thicker disk specimens tend to show dynamic elastic modulus closer to that of cylindrical specimen, and variation in data also became greater as t/r ratio became smaller.

The comparison between dynamic elastic modulus of disk and cylindrical specimens is presented in Fig. 10. In case of mortar specimens without coarse aggregate, relatively strong correlation, between dynamic elastic

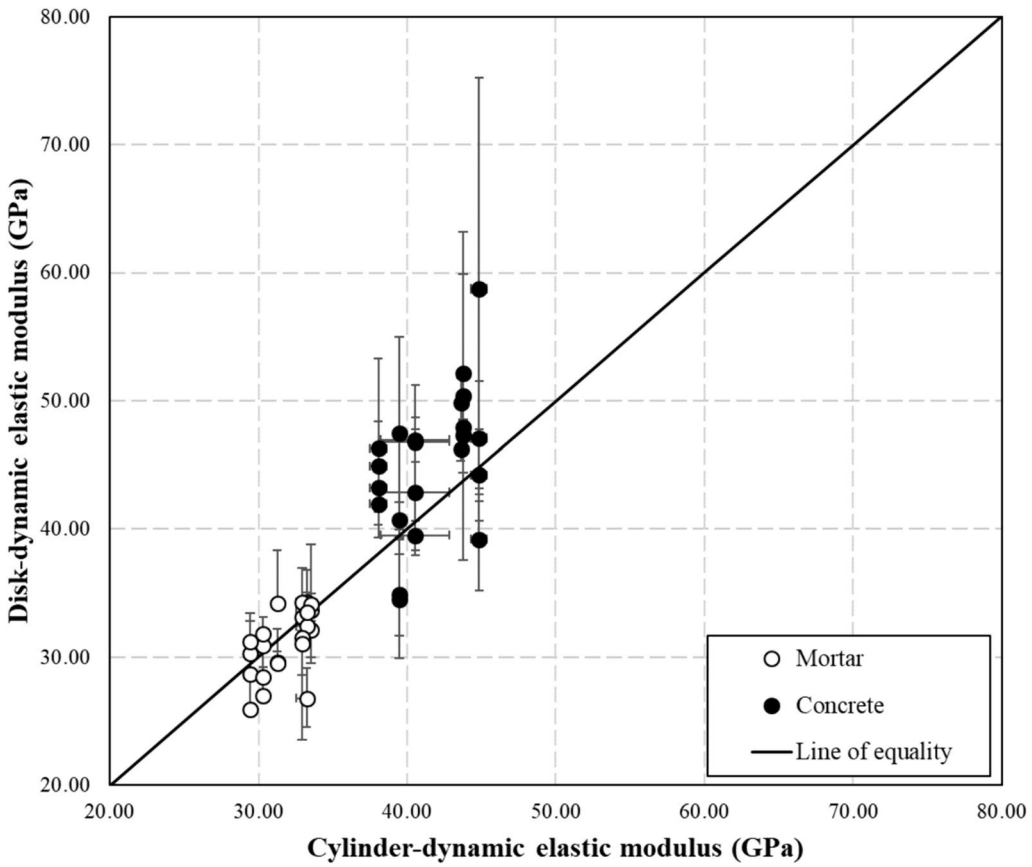

Fig. 10 Relationship between dynamic elastic modulus of disk and cylindrical concrete specimens by IR

modulus of disk and cylindrical specimen, was observed. In case of concrete specimens, disk specimens showed higher dynamic elastic modulus than cylindrical specimen. Data also showed larger variation compared to the case of mortar were observed. The reason for larger data variation can be attributed to the irregular volumetric proportion of coarse aggregate among each of the disk specimen. The reason why concrete disk specimens showed higher dynamic elastic moduli than cylindrical specimens is unclear at this moment.

3.3 Correlation Analyses

Table 7 shows results of correlation analyses. It should be noted that the value range of Pearson's correlation coefficient is from −1 to +1. The sign of the correlation coefficient indicates the direction of the relationship, and the absolute value of the coefficient indicates the strength of the relationship. The asterisk (*) that is attached to the correlation coefficient indicates that the correlation coefficient has 95% confidence level. Two asterisks indicate the confidence level of 99%, and three asterisks indicate the confidence level of 99.9%.

According to Table 7, in case of the C35 specimen measured by IET, the correlation coefficient between diameter and standard deviation was −0.5058*, and the correlation coefficient between the t/r ratio and standard deviation was −0.5065*, respectively. Since these values showed negative numbers, the relationship can be established that the standard deviation of the data decreases when the diameter of the disk specimen increases. Likewise, as t/r ratio increases, standard deviation decreases with 95% confidence level. In general, most of the factors did not present strong correlation except for the case of

Table 7 Results of correlation analysis using experimental data obtained by IET (*$p < 0.05$)

Variables	Diameter	*t/r* ratio	E_{disk}/E_{cyl}	Standard deviation
Diameter	1	0	0.1487 (C35) 0.4025* (C50) 0.3061 (M35) 0.1832 (M50)	−0.5058* (C35) −0.2004 (C50) 0.3061 (M35) 0.1832 (M50)
t/r ratio	0	1	−0.1635 (C35) −0.2742 (C50) −0.2063 (M35) −0.0208 (M50)	−0.5065* (C35) −0.5401* (C50) −0.6291* (M35) −0.5984* (M50)
E_{disk}/E_{cyl}	0.1487 (C35) 0.4025* (C50) 0.3061 (M35) 0.1832 (M50)	−0.1635 (C35) −0.2742 (C50) −0.2063 (M35) −0.0208 (M50)	1	0.3004 (C35) 0.2350 (C50) −0.064 (M35) −0.1272 (M50)
Standard deviation	−0.5058* (C35) −0.2004 (C50) 0.3061 (M35) 0.1832 (M50)	−0.5065* (C35) −0.5401* (C50) −0.6291* (M35) −0.5984* (M50)	0.3004 (C35) 0.2350 (C50) −0.064 (M35) −0.1272 (M50)	1

Table 8 Results of correlation analysis using experimental data obtained by IR (*$p < 0.05$)

Variables	Diameter	t/r ratio	E_{disk}/E_{cyl}	Standard deviation
Diameter	1	0	−0.0306 (C35) 0.6234* (C50) 0.2547 (M35) 0.2782 (M50)	−0.4608* (C35) −0.2279 (C50) −0.0593 (M35) −0.2272 (M50)
t/r ratio	0	1	−0.1358 (C35) −0.0608 (C50) 0.5428* (M35) 0.4782* (M50)	−0.5005* (C35) −0.7529* (C50) −0.3709* (M35) −0.7020* (M50)
E_{disk}/E_{cyl}	−0.0306 (C35) 0.6234* (C50) 0.2547 (M35) 0.2782 (M50)	−0.1358 (C35) −0.0608 (C50) 0.5428* (M35) 0.4782* (M50)	1	0.4102* (C35) 0.0359 (C50) 0.0507 (M35) −0.1833 (M50)
Standard deviation	−0.4608* (C35) −0.2279 (C50) −0.0593 (M35) −0.2272 (M50)	−0.5005* (C35) −0.7529* (C50) −0.3709* (M35) −0.7020* (M50)	0.4102* (C35) 0.0359 (C50) 0.0507 (M35) −0.1833 (M50)	1

t/r ratio of disk specimen and standard deviation of the data. The results of correlation analysis suggests that t/r ratio has negative correlation with standard deviation.

According to Table 8 which presents results of correlation analysis using data measured by IR, the correlation coefficient between diameter and standard deviation in C35 specimen was −0.4608*, and the correlation coefficient between the t/r ratio and standard deviation was −0.5065*, respectively. In general, t/r ratio and standard deviation showed strong negative correlation, meaning that thicker disk specimens provided smaller standard deviation in data. The difference caused by type of measurement technique (IET or IR) was not clearly identified from correlation analysis.

It is interesting to notice that the data measured by IR showed a clear trend with the increase in w/c of the specimen. As w/c ratio increased from 0.35 (C35 and M35) to 0.5 (C50 and M50), correlation coefficients between t/r ratio and standard deviation decreased from −0.5005* (C35) and −0.3709* (M35) to −0.7529* (C50) and −0.7020* (M50), respectively. The results indicate that higher w/c specimens showed higher scattering in data by the reduction of t/r ratio. In case of the data measured by IET, correlation coefficients between t/r ratio and standard deviation were −0.5065* (C35), −0.6291* (M35), −0.5401* (C50), and −0.5984* (M50), respectively. The effect caused by w/c on correlation coefficient between t/r ratio and standard deviation was not as clear as the data measured by IR. The difference between correlation coefficients were also smaller, and did not show clear trend.

It is interesting to notice that the data measured by IR showed a clear trend with the increase in w/c of the specimen. As w/c ratio increased from 0.35 (C35 and M35) to 0.5 (C50 and M50), correlation coefficients between t/r ratio and standard deviation decreased from −0.5005* (C35) and −0.3709* (M35) to −0.7529* (C50) and −0.7020* (M50), respectively. The results indicate that higher w/c specimens showed higher scattering in data by the reduction of t/r ratio. In case of the data measured by IET, correlation coefficients between t/r ratio and standard deviation were −0.5065* (C35), −0.6291* (M35), −0.5401* (C50), and −0.5984* (M50), respectively. The effect caused by w/c on correlation coefficient between t/r ratio and standard deviation was not as clear as the data measured by IR. The difference between correlation coefficients were also smaller, and did not show clear trend.

3.4 Statistical Analyses

Results from t-test are summarized in Table 9. When the diameter of the disk specimen was 50 mm, E_{disk} of M35 (t/r ratio of 0.2) measured by IR showed p value of 0.03 (smaller than 0.05), and thus determined as statistically different from E_{cyl}. It should be also noted that E_{disk} of w/c M50 (t/r ratio of 0.2) measured by IR showed p value of 0.07. Although the set of data was determined to be statistically not different from E_{cyl}, p value was so close to 0.05 that it could have almost determined as statistically different. The trend of showing low p value with M35 and M50 specimens was associated with the experimental results shown in Figs. 8 and 9. It was suspected that some level of microcrack has been generated during preparation of 5 mm thin disk specimen ($t/r = 0.2$), and thus showed higher difference between E_{cyl} and E_{disk}.

In case of the disk specimen with 75 mm diameter, E_{disk} of C35 ($t/r = 0.3$) measured by IR was found to be statistically different from E_{cyl} (showing p value of 0.04). E_{disk} of C50 ($t/r = 0.3$) also showed p value of 0.09. Except for these two sets of data, no clear statistical difference was observed between E_{cyl} and E_{disk}. With 100 mm diameter disk specimens, E_{disk} of C35 (t/r 0.3) measured by IET was found to be statistically different from E_{cyl} (showing p value of 0.03). In general, the null hypothesis used for t-test, E_{cyl} and E_{disk} were identical, and could not be rejected although such a large variation in data from disk specimen was observed from Figs. 6, 7, 8, and 9.

3.5 Discussion

Although measured dynamic elastic modulus should be theoretically identical regardless of cylindrical and disk specimens, they showed some differences. It is because (1) there is always a size effect for mechanical property measurement and (2) the effect of microcracks induced during cutting process is greater for thinner specimen (higher volume fraction of microcracks in thinner specimens). Inconsistency in measured values was also more significant when the thickness of disk specimen becomes smaller. It seems to be associated with the maximum size of aggregate in concrete, in which coarse aggregate will always be sliced with different volume fractions to cause higher variation of aggregate volume fraction in disk-shaped specimens. It should be important to notice that variation in data was also smaller in mortar specimens than concrete specimens.

For these reasons, the results from this work showed that concrete disk specimens with the diameter of 100 mm and thickness of 25 mm showed the most reliable values. It is interesting to notice that all the previous works (Dilek, 2008; Dilek & Reis, 2015; Leming et al., 1998; Park & Yim, 2016, 2017a, 2017b; Park et al., 2014; Reis & Dilek, 2013) used 100 mm×25 mm disk specimens for their works. It is not clear whether it was just a coincidence or was chosen on purpose (the reason was not clearly mentioned in their works). However, the results from this work have shown that their choice was appropriate to obtain reliable results.

Table 9 Results of the paired t-test

Specimen		Thickness/radius							
		0.5		0.4		0.3		0.2	
		P value	st.d*	*P* value	st.d*	*P* value	st.d*	*P* value	st.d*
Diameter		50							
IET method	C35	0.85	No	0.85	No	0.77	No	0.91	No
	M35	0.49	No	0.14	No	0.71	No	0.79	No
	C50	0.34	No	0.54	No	0.82	No	0.84	No
	M50	0.44	No	0.53	No	0.43	No	0.49	No
IR method	C35	0.82	No	0.48	No	0.93	No	0.70	No
	M35	0.97	No	0.59	No	0.74	No	0.03	Yes*
	C50	0.55	No	0.64	No	0.60	No	0.62	No
	M50	0.37	No	0.77	No	0.95	No	0.07	No
Diameter		75							
IET method	C35	0.14	No	0.82	No	0.30	No	0.65	No
	M35	0.84	No	0.53	No	0.61	No	0.76	No
	C50	0.54	No	0.50	No	0.09	No	0.33	No
	M50	0.27	No	0.58	No	0.39	No	0.77	No
IR method	C35	0.04	Yes*	0.61	No	0.30	No	0.81	No
	M35	0.93	No	0.81	No	0.90	No	0.76	No
	C50	0.43	No	0.30	No	0.44	No	0.60	No
	M50	0.74	No	0.61	No	0.79	No	0.82	No
Diameter		100							
IET method	C35	0.32	No	0.37	No	0.03	Yes*	0.54	No
	M35	0.77	No	0.58	No	0.94	No	0.97	No
	C50	0.89	No	0.27	No	0.37	No	0.57	No
	M50	0.75	No	0.75	No	0.89	No	0.25	No
IR method	C35	0.81	No	0.23	No	0.29	No	0.48	No
	M35	0.84	No	0.89	No	0.56	No	0.30	No
	C50	0.88	No	0.48	No	0.28	No	0.71	No
	M50	0.80	No	0.55	No	0.92	No	0.38	No

* st.d = statistical difference

It should be noted that the original purpose of the research was to reduce the radius and thickness of the disk specimen as small as possible to obtain more detailed information on depth-by-depth deterioration. At this moment, it is recommended that reduction in the diameter and thickness should be limited until the reasons for higher data variation are clearly identified. Further works need to be performed by controlling the size and proportion of the coarse aggregate, sample preparation procedure (to minimize the damage associated with sample preparation), and moisture content, etc., to suggest the smallest allowable diameter and thickness for estimation of dynamic elastic modulus from thin disk specimens.

In general, the level of variation in dynamic elastic moduli of disk specimens measured by IR were smaller than those measured by IET. Such tendency became stronger as the diameter of disk specimen became smaller. The results indicate that IR is a more reliable test procedure than IET. Moreover, the test procedure for IR is simpler and easier than that for IET. In comparison with IR and IET, it is considered that IR can be a better alternative for estimation of dynamic elastic modulus from a thin disk specimen although resonant frequency measurement of disk specimen by IR has not yet been specified in standard testing procedures, e.g., ASTM.

4 Conclusion

The decrease in dynamic elastic modulus is a primary quantitative indicator of damage in concrete; hence, the depth-wise damage within a concrete structure can be quantitatively assessed using disk shapes concrete specimen fabricated from cylindrical concrete specimen obtained by coring. For higher resolution in depth-based

damage assessment, fabricating disk specimens with the thinnest possible thickness is necessary for measuring the dynamic modulus.

In order investigate the reliability and variability of dynamic elastic modulus measurement using smaller sized specimens, the dynamic elastic modulus of disk specimens with varying thicknesses and diameters, made from concrete and mortar with different water-to-cement ratios, was measured using the IET and IR methods. The dynamic elastic modulus measured using disk specimens appeared to be similar to that measured using cylinder specimens. However, the degree of similarity and variability differ based on factors such as the thickness-to-radius ratio of the disk specimen, diameter, water-to-cement ratio, and the presence of coarse aggregates. Based on the measurements of the dynamic elastic modulus of the disk specimens, the following conclusions can be drawn:

1) The level of variation in dynamic elastic moduli of disk specimen measured by IR was smaller than those measured by IET. Such tendency became stronger as the diameter of disk specimen became smaller.
2) The variability in the dynamic elastic modulus of mortar specimens, which has no coarse aggregates, is lower compared to concrete specimens.
3) The thicker disk specimens of both concrete and mortar tend to show dynamic elastic modulus closer to that of cylindrical specimens.
4) The variability in the measured dynamic elastic modulus decreases as the thickness-to-radius ratio (t/r) of the disk specimens increases, and as the diameter of the specimens increases.

Acknowledgements
Not applicable.

Author contributions
MSK: investigation, writing—original draft preparation. JJS: investigation, writing—original draft preparation. CWC: conceptualization, writing—reviewing and editing. CJL: conceptualization, methodology, writing—reviewing and editing.

Funding
This work was supported by the Energy R&D Program of the Korea Institute of Energy Technology Evaluation and Planning (KETEP) granted financial resource from the Ministry of Trade, Industry & Energy, Republic of Korea (No.20217910100100)

Availability of data and materials
The data sets used for the current study are available from the corresponding authors on reasonable request.

Declarations

Ethics approval and consent to participate
Not applicable.

Consent for publication
I, Chang Joon Lee, grant permission for the publication of my manuscript titled "Factors Influencing Measurement of Dynamic Elastic Modulus from Disk-Shaped Concrete Specimen" in IJCSM. I confirm that all the co-authors are informed and agree to the submission. The manuscript is original, and I commit to timely cooperation for any revisions during the editorial process. Date: 28th Jan 2024, Chang Joon Lee.

Competing interests
The authors declare that they have no competing interests.

Received: 28 January 2024 Accepted: 26 June 2024
Published online: 04 October 2024

References

Abu Shanab, I., & Sorensen, A. D. (2023). Improved removal efficiency of partial bridge deck repair patches using the saw and patch method. *Journal of Structural Integrity and Maintenance*. https://doi.org/10.1080/24705314.2023.2253068

Alarcon-Ruiz, L., Platret, G., Massieu, E., & Ehrlacher, A. (2005). The use of thermal analysis in assessing the effect of temperature on a cement paste. *Cement and Concrete Research, 35*(3), 609–613. https://doi.org/10.1016/j.cemconres.2004.06.015

Alqassim, M. A., Jones, M. R., Berlouis, L. E. A., & Daeid, N. N. (2016). A thermo-analytical, X-ray diffraction and petrographic approach to the forensic assessment of fire affected concrete in the United Arab Emirates. *Forensic Science International, 264*, 82–88. https://doi.org/10.1016/j.forsciint.2016.03.015

AMERICAN SOCIETY FOR TESTING AND MATERIALS. (2019). ASTM C-215: Standard test method for fundamental transverse, longitudinal and torsional frequencies of concrete specimens. *American Society for Testing and Material, 04*(02), 7p. https://doi.org/10.1520/C0215-19

AMERICAN SOCIETY FOR TESTING AND MATERIALS. (2022). ASTM E 1876–22: Standard test method of dynamic young's modulus, shear modulus, and Poisson's ratio by impulse excitation of vibration. *American Society for Testing and Materials, 03*(01), 19p. https://doi.org/10.1520/E1876-22

Bang, E. S., Park, S. G., & Kim, D. S. (2013). Evaluating shear wave velocity of rock specimen through compressional wave velocities obtained from ffrc and ultrasonic velocity methods. *Korean Society of Earth and Exploration Geophysicists., 16*(4), 250–256. https://doi.org/10.7582/GGE.2013.16.4.250

Bharatkumar, B. H., Narayanan, R., Raghuprasad, B. K., & Ramachandramurthy, D. S. (2001). Mix proportioning of high performance concrete. *Cement and Concrete Composites, 23*(1), 71–80. https://doi.org/10.1016/S0958-9465(00)00071-8

Byun, Y., & Ryu, D. (2017). an experimental study on the diagnosis and evaluation of damage characteristics of fire damaged concrete by strength level: In relation to carbonation depth. *Journal of the Korean Society of Hazard Mitigation, 17*(6), 533–539. https://doi.org/10.9798/KOSHAM.2017.17.6.19

Chen, F., Gao, C., Jin, L., Du, X., Bary, B., Le Pape, Y., & Sanahuja, J. (2023). Numerical investigations on the viscoelastic-damage behaviors of RIVE-induced concrete. *International Journal of Mechanical Sciences, 239*, 107899. https://doi.org/10.1016/j.ijmecsci.2022.107899

Dilek, U. (2008). Assessment of damage gradients using dynamic modulus of thin concrete disks. *ACI Materials Journal, 105*(5), 49.

Dilek, U., & Reis, E. (2015). Comparison of nondestructive evaluation findings, constrained and unconstrained wave speeds, dynamic moduli, and Poisson's ratio of core specimens from a concrete structure damaged by fire. *Journal of Performance of Constructed Facilities, 29*(5), 04014136. https://doi.org/10.1061/(ASCE)CF.1943-5509.000054

Du, S., Zhang, Y., Sun, Q., Gong, W., Geng, J., & Zhang, K. (2018). Experimental study on color change and compression strength of concrete tunnel lining in a fire. *Tunnelling and Underground Space Technology, 71*, 106–114. https://doi.org/10.1016/j.tust.2017.08.025

Dvořák, R., Chobola, Z., Plšková, I., Hela, R., & Bodnárová, L. (2023). (2023) Classification of thermally degraded concrete by acoustic resonance method and image analysis via machine learning. *Materials, 16*(3), 1010. https://doi.org/10.3390/ma16031010

Georgali, B., & Tsakiridis, P. E. (2005). Microstructure of fire-damaged concrete. A case study. *Cement and Concrete Composites, 27*(2), 255–259. https://doi.org/10.1016/j.cemconcomp.2004.02.022

Gharehbaghi, V. R., Kalbkhani, H., Noroozinejad Farsangi, E., Yang, T. Y., Nguyen, A., Mirjalili, S., & Málaga-Chuquitaype, C. (2022). A novel approach for deterioration and damage identification in building structures based on Stockwell-Transform and deep convolutional neural network. *Journal of Structural Integrity and Maintenance, 7*(2), 136–150.

Ghodousian, O., Garcia, R., Shafaie, V., & Ghodousian, A. (2023). Interfacial bond strength of coloured SCC repair layers: An experimental and optimisation study. *Journal of Structural Integrity and Maintenance*. https://doi.org/10.1080/24705314.2023.2170620

Ha, T., Ko, J., Lee, S., Kim, S., Jung, J., & Kim, D. J. (2016). A case study on the rehabilitation of a fire-damaged structure. *Applied Sciences, 6*(5), 126. https://doi.org/10.3390/app6050126

Hua, N., Khorasani, N. E., Tessari, A., & Ranade, R. (2022). Experimental study of fire damage to reinforced concrete tunnel slabs. *Fire Safety Journal, 127*, 103504. https://doi.org/10.1016/j.firesaf.2021.103504

Hutchinson, J. R. (1979). "Axisymmetric flexural vibrations of a thick free circular plate. *ASME J Appl Mech, 46*(1), 139–144. https://doi.org/10.1115/1.3424485

Ingham, J. P. (2009). Application of petrographic examination techniques to the assessment of fire-damaged concrete and masonry structures. *Materials Characterization, 60*(7), 700–709. https://doi.org/10.1016/j.matchar.2008.11.003

Kirchhof, L. D., Lorenzi, A., & Silva Filho, L. C. P. (2015). Assessment of concrete residual strength at high temperatures using ultrasonic pulse velocity. *The e-Journal of Nondestructive Testing, 20*(7), 1–9.

Krishna, D. A., Priyadarsini, R. S., & Narayanan, S. (2019). Effect of elevated temperatures on the mechanical properties of concrete. *Procedia Structural Integrity, 14*, 384–394. https://doi.org/10.1016/j.prostr.2019.05.047

Lee, B. J., Kee, S. H., Oh, T. K., & Kim, Y. Y. (2017). Evaluating the dynamic elastic modulus of concrete using shear-wave velocity measurements. *Advances in Materials Science and Engineering., 2017*(5), 1–13. https://doi.org/10.1155/2017/1651753

Lee, J. C., Lee, C. J., Kim, W. J., & Lee, J. H. (2015). Characteristics of elastic wave in fire damaged high strength concrete using impact-echo method. *Fire Science and Engineering, 29*(1), 1–6. https://doi.org/10.7731/KIFSE.2015.29.1.001

Leming, M. L., Nau, J. M., & Fukuda, J. (1998). Non-destructive determination of the dynamic modulus of concrete disks. *Materials Journal, 95*(1), 50–57. https://doi.org/10.14359/353

Li, Q., Li, Z., Yuan, G., & Shu, Q. (2013). The effect of a proprietary inorganic coating on compressive strength and carbonation depth of simulated fire-damaged concrete. *Magazine of Concrete Research, 65*(11), 651–659. https://doi.org/10.1680/macr.12.00119

Li, Q., Yuan, G., & Shu, Q. (2014). Effects of heating/cooling on recovery of strength and carbonation resistance of fire-damaged concrete. *Magazine of Concrete Research, 66*(18), 925–936. https://doi.org/10.1680/macr.14.00029

Li, S., Yu, X., Yang, S., Wang, H., & Chen, D. (2023). A micromechanical-based semi-empirical model for predicting the compressive strength degradation of concrete under external sulfate attack. *Materials, 16*(16), 5542. https://doi.org/10.3390/ma16165542

Lim, G. S., Han, S. H., Han, J. H., Yoon, C. W., Han, M. C., Han, C. G. (2021). Assessment of fire damage of 21 MPa-class concrete using thermogravimetric analysis. Proceedings of the Korean Institute of Building Construction Conference; 2021 May 20–21; Shinwha World, Jeju, Republic of Korea. Seoul (Republic of Korea): The Korea Institute of Building Construction. 243–244. Retrived from https://kiss.kstudy.com/Detail/Ar?key=3887834

Ma, Q., Guo, R., Zhao, Z., Lin, Z., & He, K. (2015). Mechanical properties of concrete at high temperature—a review. *Construction and Building Materials, 93*, 371–383. https://doi.org/10.1016/j.conbuildmat.2015.05.131

Martinček, G. (1965). The determination of Poisson's ratio and the dynamic modulus of elasticity from the frequencies of natural vibration in thick circular plates. *Journal of Sound and Vibration, 2*(2), 116–127. https://doi.org/10.1016/0022-460X(65)90089-1

Mendes, A., Sanjayan, J. G., & Collins, F. (2009). Long-term progressive deterioration following fire exposure of OPC versus slag blended cement pastes. *Materials and Structures, 42*, 95–101. https://doi.org/10.1617/s11527-008-9369-7

Mitchell, S. J., Pandolfi, A., & Ortiz, M. (2014). Metaconcrete: Designed aggregates to enhance dynamic performance. *Journal of the Mechanics and Physics of Solids, 65*, 69–81. https://doi.org/10.1016/j.jmps.2014.01.003

Nilsen, A. U., & Monteiro, P. J. (1993). Concrete: A three phase material. *Cement and Concrete Research, 23*(1), 147–151. https://doi.org/10.1016/0008-8846(93)90145-Y

Park, G. K., & Yim, H. J. (2017b). Evaluation of fire-damaged concrete: An experimental analysis based on destructive and nondestructive methods. *International Journal of Concrete Structures and Materials, 11*(3), 447–457. https://doi.org/10.1007/s40069-017-0211-x

Park, S. J., & Yim, H. J. (2016). Evaluation of residual mechanical properties of concrete after exposure to high temperatures using impact resonance method. *Construction and Building Materials, 129*, 89–97. https://doi.org/10.1016/j.conbuildmat.2016.10.116

Park, S. J., & Yim, H. J. (2017a). Evaluation of material properties of fire-damaged concrete under post-fire curing regimes using impact resonance vibration method. *Journal of the Korea Institute for Structural Maintenance and Inspection, 21*(5), 42–48. https://doi.org/10.11112/jksmi.2017.21.5.042

Park, S. J., Yim, H. J., & Kwak, H. G. (2014). Nonlinear resonance vibration method to estimate the damage level on heat-exposed concrete. *Fire Safety Journal, 6*(69), 36–42. https://doi.org/10.1016/j.firesaf.2014.07.003

Pathak, R. P., Munzni, B. K., Sharma, P., Mahure, N. V., Vyas, S., & Ratnam, M. (2013). Estimation of fire damage to concrete structure: A case study. *International Journal of Engineering, 2*(4), 130–136.

Reis, E. M., & Dilek, U. (2013). Non-destructive evaluation and laboratory testing of a concrete structure damaged by fire. In Forensic Engineering 2012: Gateway to a Safer Tomorrow. 1159–1166. https://doi.org/10.1061/9780784412640.123

Shah, M. U., Usman, M., Khushnood, R. A., & Hanif, A. (2023). Diagnosis of durability-related problems in concrete structures through comprehensive analysis and non-destructive testing: A case study. *Journal of Structural Integrity and Maintenance*. https://doi.org/10.1080/24705314.2023.2233812

Sim, S. R., & Ryu, D. W. (2020). A method for instant estimation of the temperature experienced by fire-damaged reinforced concrete structures using titanium. *Materials, 13*(8), 1993. https://doi.org/10.3390/ma13081993

Thanaraj, D. P., Anand, N. G. P. A., Prince Arulraj, G., & Zalok, E. (2020). Post-fire damage assessment and capacity based modeling of concrete exposed to elevated temperature. *International Journal of Damage Mechanics, 29*(5), 748–779. https://doi.org/10.1177/1056789519881484

The Math Works, Inc. (2020). MATLAB. Version 2020a, The Math Works, Inc. Computer Software. www.mathworks.com/

Yang, H., Lin, Y., Hsiao, C., & Liu, J. Y. (2009). Evaluating residual compressive strength of concrete at elevated temperatures using ultrasonic pulse velocity. *Fire Safety Journal, 44*(1), 121–130. https://doi.org/10.1016/j.firesaf.2008.05.003

Ye, G., Liu, X., De Schutter, G., Taerwe, L., & Vandevelde, P. (2007). Phase distribution and microstructural changes of self-compacting cement paste at elevated temperature. *Cement and Concrete Research, 37*(6), 978–987. https://doi.org/10.1016/j.cemconres.2007.02.011

Yoon, Y., Lee, J., Choi, H., & Oh, T. (2021). A study on the detection of internal defect types for duct depth of prestressed concrete structures using electromagnetic and elastic waves. *Materials, 14*(14), 3931. https://doi.org/10.3390/ma14143931

Zhang, S., Zhang, C., Liao, L., & Wang, C. (2018). Numerical study of the effect of ITZ on the failure behaviour of concrete by using particle element modelling. *Construction and Building Materials, 170*, 776–789. https://doi.org/10.1016/j.conbuildmat.2018.03.040

Zhou, X., Xie, Y., Long, G., Zeng, X., Li, J., Yao, L., & Pan, Z. (2021). DEM analysis of the effect of interface transition zone on dynamic splitting tensile behavior of high-strength concrete based on multi-phase model. *Cement and Concrete Research, 149*, 106577. https://doi.org/10.1016/j.cemconres.2021.106577

Min Suk Kim M.E., Department of Architectural Engineering, Chungbuk National University, Chungdae-ro 1, Seowon-gu, Cheongju, Chungcheongbuk-do, 28644, Republic of Korea.

Jeong Jin Son B.E., Master Student, Division of Architectural and Fire Protection Engineering, Pukyong National University, Yongso-ro 45, Nam-gu, Busan, 48513, Republic of Korea.

Chul-Woo Chung Ph.D, Professor, Division of Architectural and Fire Protection Engineering, Pukyong National University, Yongso-ro 45, Nam-gu, Busan, 48513, Republic of Korea.

Chang Joon Lee Ph.D, Professor, Corresponding Author, Chungbuk National University, Chungdae-ro 1, Seowon-gu, Cheongju, Chungcheongbuk-do, 28644, Republic of Korea.